Synlett K. Kumar et al. Letter

Dissymmetric *Bay*-Functionalized Perylenediimides

Kapil Kumar[a]
Gaurav Bhargava[b]
Subodh Kumar[a]
Prabhpreet Singh*[a]

[a] Department of Chemistry, UGC Centre for Advanced Studies, Guru Nanak Dev University, Amritsar 143 005, India
prabhpreet.chem@gndu.ac.in
[b] Department of Chemical Sciences, IK Gujral Punjab Technical University, Kapurthala-144601, Punjab, India

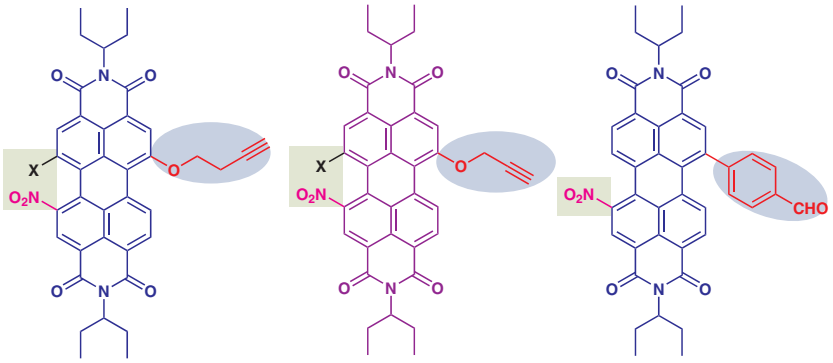

Received: 29.03.2018
Accepted after revision: 17.05.2018
Published online: 20.06.2018
DOI: 10.1055/s-0037-1610186; Art ID: st-2018-u0190-l

Abstract We report the synthesis of perylenediimide (PDI)-based donor–acceptor hybrids through dissymmetric *bay* functionalization of PDIs. The dissymmetric *bay*-functionalized di- and trisubstituted PDIs were characterized by using one- and two-dimensional NMR spectroscopy. Density functional theory calculations revealed (i) an energy gap between the HOMO and LUMO in the range 2.14–2.34 eV, beneficial for charge-transfer properties; and (ii) a twist angle between the two naphthalene units in the range 17–26°, which might be beneficial for disruption of co-facial stacking of the PDI.

Key words perylenediimide, dissymmetric functionalization, *bay* functionalization, nitration, density functional theory

Perylenediimide[1–4] (PDI), an important member of the rylene family, is a promising scaffold owing to the prominent features of PDIs such as their excellent optical, chemical, and thermal robustness; high fluorescence quantum yield; high electron mobility; and high molar absorptivity. Moreover, the optical, electronic, and aggregation properties of PDIs can be modified by judicious selection of functional groups at the *N*-imide, *bay*, *ortho*, or *peri* positions of the PDI core.[2–6] Therefore, PDIs have been explored for various applications in the dye and pigment industries[5] and in optoelectronic devices.[6–10] Recently, *bay*- and N-terminal-functionalized PDIs have been explored in supramolecular chemistry.[11–17] In this context, PDI-based chromophores with attached donor and acceptor substituents (D–A hybrids) might be potential candidate for use as reaction-based probes for producing long-wavelength-absorbing dyes[18] and in the field of organic photovoltaic devices.[19]

In literature reports, basically, either two (1,7-) or four (1,6,7,12-) positions of the *bay* area of PDIs (**A**, Scheme 1) have been extensively used for homogeneous functionalization through nucleophilic substitution or Suzuki/Sonogashira coupling reactions of di- or tetrahalogenated derivatives in the presence or absence of a catalyst, to attach various aryl or alkyl groups to the PDI core (**B** and **C**; Scheme 1).[1–6] PDIs with two different functional groups in the *bay* positions can be prepared by multiple stepwise substitution reactions of halogenated PDIs, but these syntheses involve cumbersome purification procedures and give the desired product in low to moderate yield (**D**; Scheme 1).[20] Few reports have appeared that discusses halogenated or non-halogenated routes for the synthesis of dissymmetric *bay*-functionalized di- or trisubstituted PDIs (**E**; Scheme 1). We therefore proposed that PDI-based D–A hybrids might be synthesized by dissymmetric *bay* functionalization of the PDI core.[21]

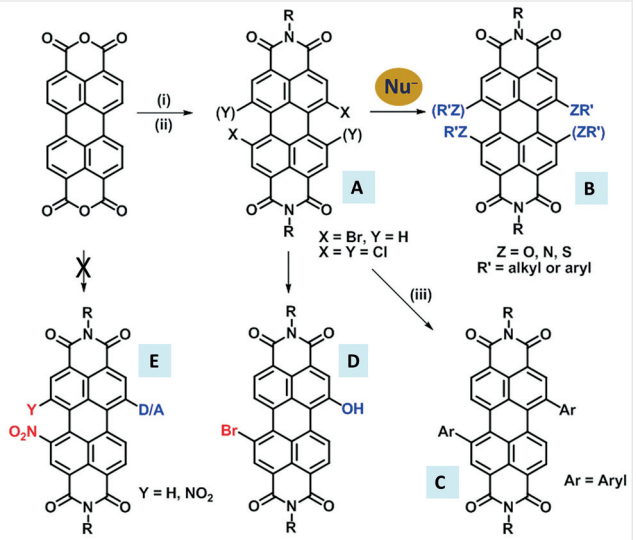

Scheme 1 General approaches for the synthesis of dissymmetric functionalized PDIs reported in the literature

In continuation of our interest in developing PDI- and pyrimidinone-based receptors for applications in supramolecular chemistry,[22] we report the design, synthesis, and characterization of dissymmetric *bay*-functionalized di- and trisubstituted PDIs through controlled nitration of monosubstituted PDIs (Figure 1). Density functional theory (DFT) calculations, NMR spectroscopy, electrochemical studies, and UV-vis spectroscopy were used to elucidate the electronic and optical behaviors of PDIs **1**–**5**.

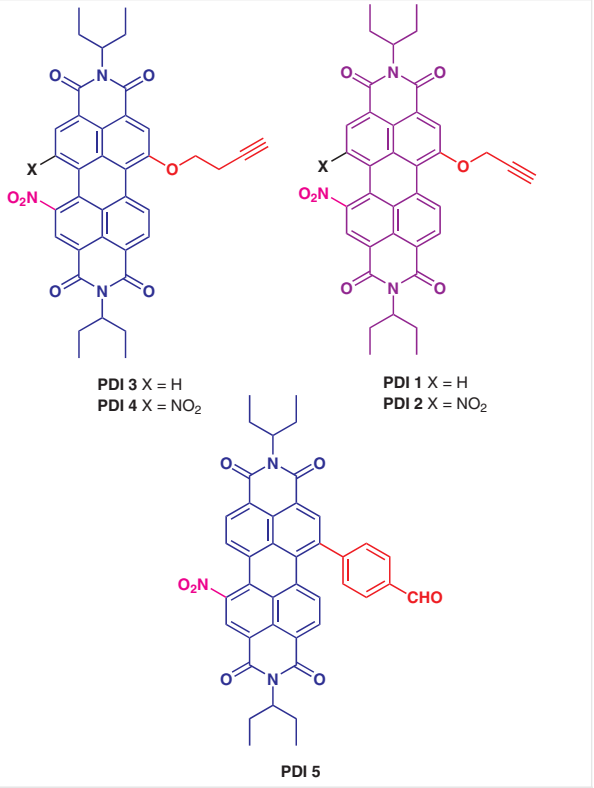

Figure 1 Chemical structures of dissymmetric *bay*-functionalized PDIs **1**–**5**

We synthesized PDIs **6**, **7**, and **9** (Scheme 2) by following the procedures reported in the literature.[12,23] Ceric ammonium nitrate (CAN)-mediated nitration of PDI **6** was accomplished in presence of a H_2SO_4–HNO_3 mixture to give PDI **8**. We observed that stabilization of the nitrating species in H_2SO_4 during nitration of PDI **6** at room temperature drastically reduced the reaction time to 10–15 min (in comparison to the two hours reported in the literature),[23] and gave PDI **8** in >90% yield.

With these encouraging results, we extended our nitration method to the preparation of dissymmetric *bay*-functionalized di- and trisubstituted PDIs. For this purpose PDI **9** was subjected to nitration at room temperature by using a similar protocol with a nitrating mixture consisting of CAN (1.0 equiv), HNO_3 (16.9 equiv), and H_2SO_4 (18.9 equiv).[24] Immediately, we observed the formation of a blue-colored product that moved faster on TLC (R_f = 0.4) with respect to PDI **9** (R_f = 0.3) (Scheme 2). In the ^{1}H NMR spectrum of this blue-colored product, we observed the presence of two singlets at δ = 9.14 and 8.87 ppm and one doublet at δ = 8.32 ppm, corresponding to 1 H each, clearly separated out, together with one doublet and one singlet of 1 H each at δ = 8.55–8.57 ppm that merged with one another [see Supplementary Information (SI); Figures S3 and S4]. In the proton–carbon heteronuclear correlation (HSQC) spectrum, we observed five hydrogen atoms of the perylene aromatic core corresponding to five carbon signals in the aromatic region (SI; Figure S3f). These NMR data indicate that PDI **9** undergoes nitration at two positions to form the dissymmetric trifunctionalized PDI **2**[25] (Scheme 2).

We further surmised that controlled and careful nitration of PDI **9** through portionwise addition and equivalency of the nitrating mixture might result in the formation of a disubstituted product with nitration at only one position. We therefore attempted another reaction with a nitrating mixture consisting of CAN (0.47 equiv), H_2SO_4 (2.47 equiv), and HNO_3 (5.64 equiv).[26] On monitoring the progress of the reaction by TLC, we observed a new purple-colored spot at R_f = 0.26, compared with PDI **2** (R_f = 0.4) (Scheme 2). We successfully purified this compound through column chromatography [silica gel, $CHCl_3$–hexane (7:3)] in 90% yield; PDI **2** was also isolated in <3% yield. The ^{1}H NMR spectrum of the product showed two singlets of 1 H each at δ = 8.51 and 9.04 ppm, and two doublets of 1 H each at δ = 8.68 and 8.78 ppm (SI; Figures S4 and S5); two doublets of 2 H protons each merged with one another at δ = 8.64 ppm. The presence of six correlations in the HSQC, corresponding to six ArC–H signals (SI; Figure S5) led us to conclude that the dissymmetric disubstituted product PDI **1**[27] had been formed (Scheme 2).

The series of dissymmetric substituted PDIs was further expanded by the synthesis of the butyne-linked derivatives PDI **3**[28] and PDI **4**[29] (Scheme 2, left). The PDI **10** was synthesized from PDI **7** through nucleophilic substitution with but-1-yn-1-ol in the presence of a K_2CO_3–DMF mixture (SI; Figure S6). In the ^{1}H NMR spectrum, the presence of two triplets at δ = 4.63 ppm (due to –OCH_2) and δ = 2.22 ppm (due to –CH), and of a triplet of doublets at δ = 3.00 ppm (due to –CH_2), along with the requisite signals of the PDI core indicated that PDI **10** had been formed. Subsequently, PDI **10** was subjected to nitration, under similar conditions to those described above, to give PDIs **3** and **4**. The purity and structures of PDIs **3** and **4** were established by NMR techniques (^{1}H and ^{13}C NMR spectra and HSQC) (SI; Figure S7 and S8).

To widen the scope the method and to expand the series of dissymmetric substituted PDIs, PDI **5**[30] was synthesized (Scheme 3). To synthesize PDI **5**, we first performed a Suzuki coupling of PDI **7** with (4-formylphenyl)boronic acid in the presence of $Pd(PPh_3)_4$ in toluene to give PDI **11** (SI; Figure S9). Subsequently, PDI **11** was subjected to nitration with

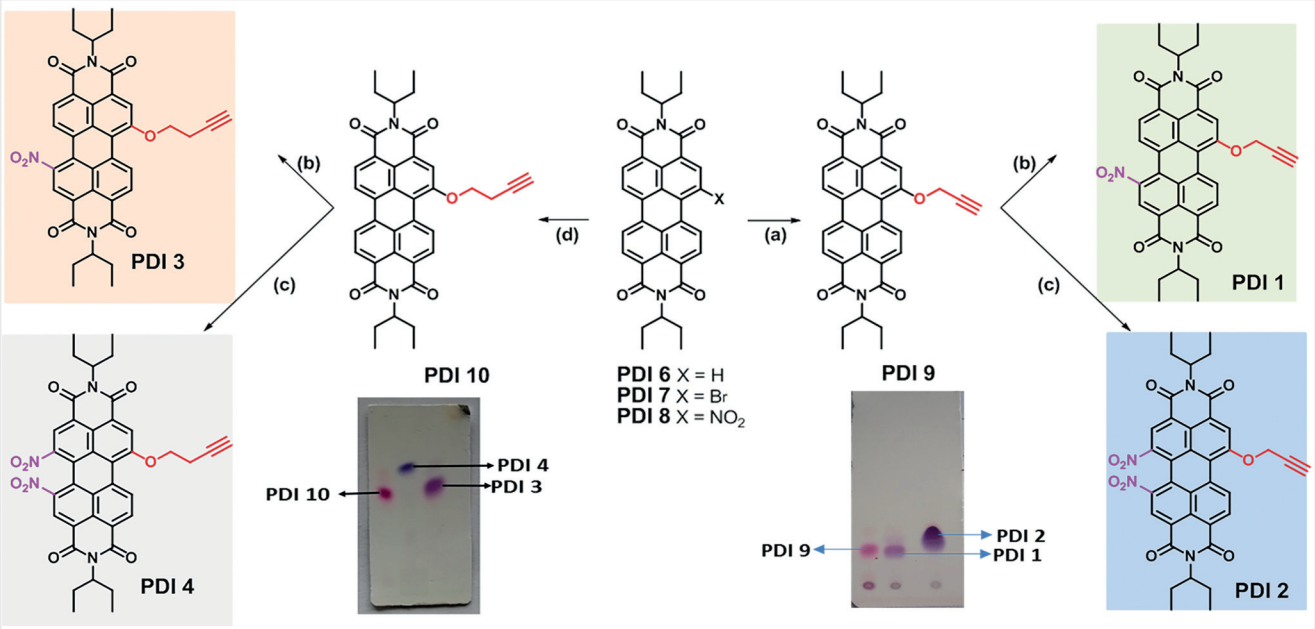

Scheme 2 Synthesis of dissymmetric *bay*-substituted perylenediimides; *Reagents and conditions*: (a) propargyl alcohol, K_2CO_3, DMF, 9 h, 90 °C; (b) HNO_3 (5.64 equiv), CAN (0.47 equiv), H_2SO_4 (2.47 equiv), r.t., 4 h; (c) HNO_3 (16.9 equiv), CAN (1.0 equiv), H_2SO_4 (18.9 equiv), r.t., 10 h; (d) but-1-yn-1-ol, K_2CO_3, DMF, 9 h, 90 °C.

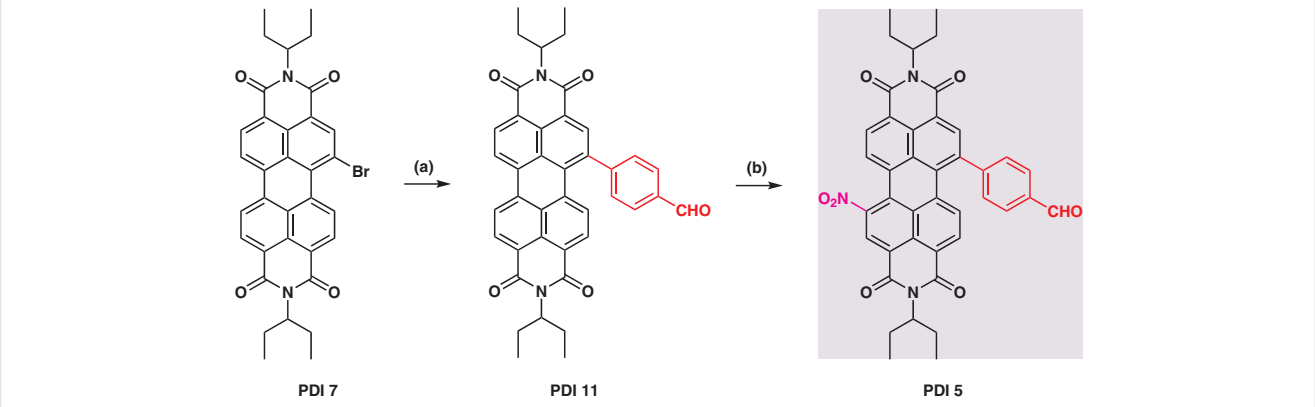

Scheme 3 Synthesis of dissymmetric *bay*-substituted perylenediimide **5**; *Reagents and conditions*: (a) (4-formylphenyl)boronic acid, $Pd(PPh_3)_4$, toluene, 12 h, 80 °C; (b) HNO_3 (5.64 equiv), CAN (0.47 equiv), H_2SO_4 (2.47 equiv), r.t., 4 h.

CAN (0.47 equiv), H_2SO_4 (2.47 equiv), and HNO_3 (5.64 equiv) to give the disubstituted PDI **5** (Scheme 3 and SI; Figure S10).

Unfortunately, even after repeated attempts, we were unable to isolate any trisubstituted PDI derivatives. The electron-withdrawing nature of the formylbenzene group in the *bay* position of the PDI inhibits the formation of trisubstituted PDI derivatives containing two nitro groups.

The purity and structure of PDI **5** were established by ^1H and ^{13}C NMR spectroscopy. Interestingly, oxidation of the –CHO group to a –COOH group was not observed during nitration of PDI **11** (the resonance signal of the -CHO proton appeared as singlet at δ = 10.51 in PDI **5**). PDI **5** might therefore be a potential candidate for various applications after performing desired functionalizations at one or both of the –CHO and $–NO_2$ groups.

To obtain insight into the effects of the presence of dissymmetric substituents in the *bay* positions on the electronic properties of PDIs, the molecular structures of PDIs **1**–**5** were optimized at the B3LYP/6-31G* level by using density functional theory (DFT) (Figures 2 and 3 and Table 1). In PDIs **1**–**4**, we expected that the presence of the propargyloxy or but-1-ynyloxy groups would enrich the electron density, whereas the presence of the $–NO_2$ groups

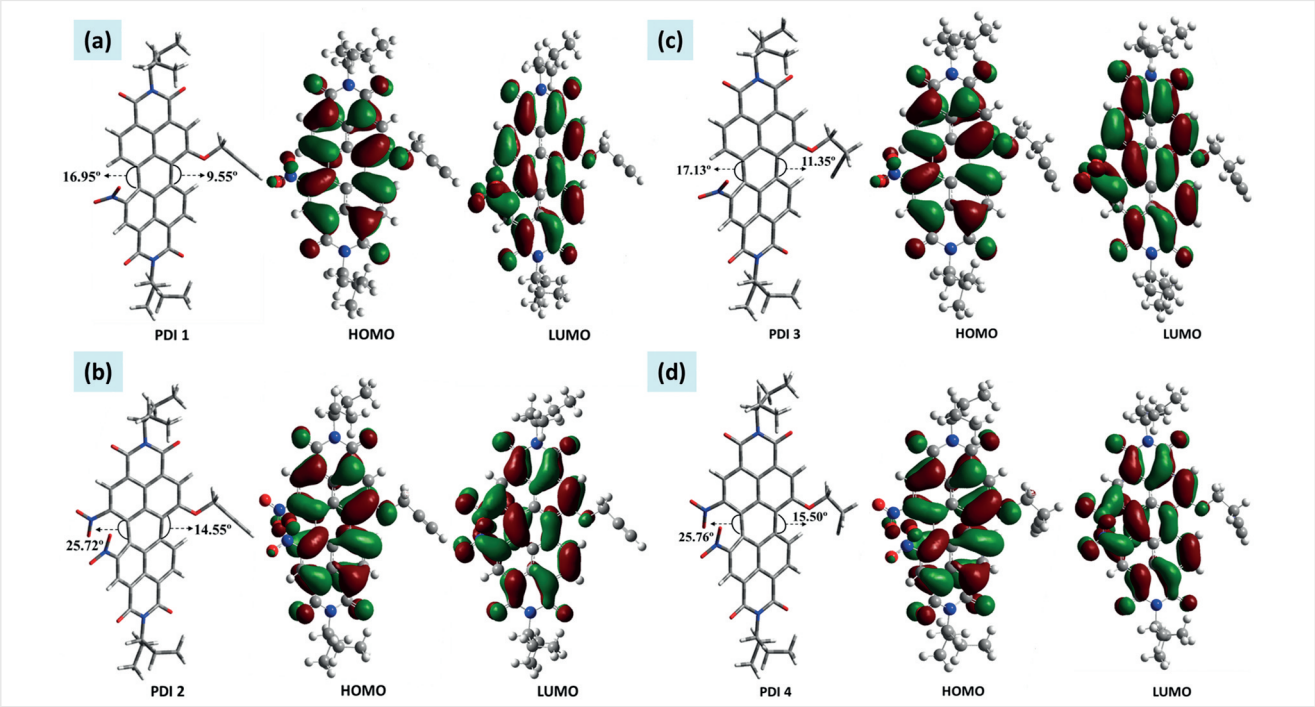

Figure 2 The optimized structures of PDI **1–4** (a–d; left) calculated by DFT at the B3LYP/6-31G* level. The dihedral angles and a representation of the computed frontier molecular orbitals (HOMOs and LUMOs) of the PDIs **1–4** are shown (a–d; right).

would induce electron deficiency in the perylene core. From molecular orbital analysis, we observed that the HOMOs are localized on the central PDI moiety and on the donor oxygen atom of the –OR (R = propargyl or but-1-ynyl) moiety, whereas the LUMO is extended uniformly from the PDI moiety to the nitro moieties (Figure 2). The LUMO and HOMO levels of PDI **1** drop to –3.86 from –3.46 eV (PDI **9**) and to –6.19 from –5.84 eV (PDI **9**), respectively. As expected, the presence of two nitro groups in the *bay* positions in PDI **2** results in a further decrease in the HOMO level to –6.47 eV, whereas drastic decrease in the LUMO level to –4.32 eV in comparison to PDI **9** occurs (Figure 3 and Table 1). A similar trend was observed on moving from PDI **10** to PDI **3** to PDI **4**.

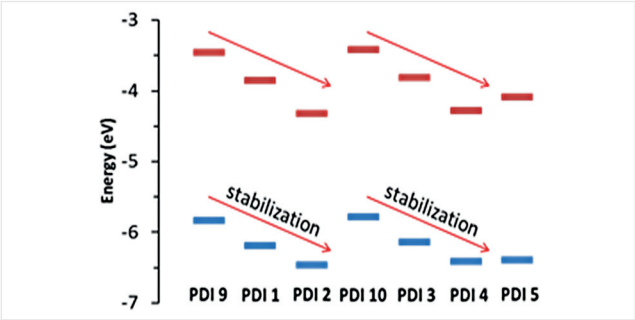

Figure 3 General representation of the energy levels (HOMOs and LUMOs) for PDIs **1–5** calculated by DFT with the B3LYP/6-31G* basis set. Blue and red bars represent the HOMO and LUMO levels (in eV), respectively.

Table 1 Calculated and Experimental Parameters for PDIs **1–5**

Compound	Calculated by DFT (B3LYP/6-31G*)			Calculated by cyclic voltammetry			Angles of twist (°)	λ_{max} (nm)
	HOMO (eV)	LUMO (eV)	E_g (eV)	HOMO (eV)	LUMO (eV)	E_g (eV)		
PDI 9	–5.84	–3.46	2.30	–5.94	–3.55	2.39	1.0, 1.1	531
PDI 1	–6.19	–3.86	2.33	–6.16	–3.88	2.28	9.6, 17.0	541
PDI 2	–6.47	–4.32	2.14	–6.18	–3.96	2.22	14.5, 25.7	554
PDI 10	–5.79	–3.42	2.37	–5.90	–3.54	2.36	7.1, 4.4	536
PDI 3	–6.14	–3.82	2.32	–6.25	–3.83	2.42	11.3, 17.1	538
PDI 4	–6.42	–4.28	2.13	–6.03	–3.90	2.13	15.5, 25.8	556
PDI 5	–6.40	–4.09	2.31	–6.11	–3.99	2.12	16.0, 23.0	525

When the propargyloxy group was replaced with a formylbenzene group in PDI **5**, the LUMO level increased to –4.09 eV in comparison to PDI **4**, indicating minor destabilization. The energy gap (E_g) between the HOMO and LUMO levels of PDIs **2** and **4** are ~2.14 eV, which is lower than those of PDIs **9**/**1** and **10**/**3**. Structure optimization of the ground-state molecular structures of the dissymmetric *bay*-substituted PDIs **1**–**5** also revealed that the two naphthalene rings of the PDI moiety have different twist angles to compensate for the strain caused by the presence of di-or trisubstitution at the *bay* positions of the PDI moiety. In the trisubstituted derivatives **2** and **4**, the approximate dihedral angles between the two naphthalene rings are 25.7°, whereas for the disubstituted derivatives **1** and **3**, the dihedral angles between the two naphthalene rings are about 17° (Figure 3). Similarly, the dihedral angle for PDI **5** is 18.0° (SI; Figure S11). These results suggest that PDIs **1**–**5** have a nonplanar structure in comparison to PDIs **9** and **10** (SI; Figures S12–16).

The electrochemical response of dissymmetric functionalized PDI **1**–**5** were also investigated by cyclic voltammetry (CV) in dichloromethane (vs. Ag/AgCl) (SI; Figure S17). The LUMO and HOMO energy levels of PDIs **1**–**5** were calculated from the cyclic voltammograms of the respective compounds by using the equation E_{LUMO}= –[E_{red}(onset) + 4.4] eV and E_{HOMO} = –[E_{ox}(onset) + 4.4] eV;[31] the results are given in Table 1. The LUMO and HOMO energy levels calculated by DFT agreed with those determined experimentally by CV.

The absorption spectra of PDIs **1**–**5**, **9**, and **10** were recorded in MeCN (Figure 4). Significant differences were observed in the absorption spectra of PDIs **1**–**5** compared with those of PDIs **9** and **10**. Broadening, along with loss of vibronic structures of the absorption spectra, were observed in cases of PDIs **1**–**5**, and the absorption maxima of PDIs **2** and **4** appeared at 554 and 556 nm, showing bathochromic shift of 23 and 20 nm in comparison to PDIs **9** and **10**, respectively.

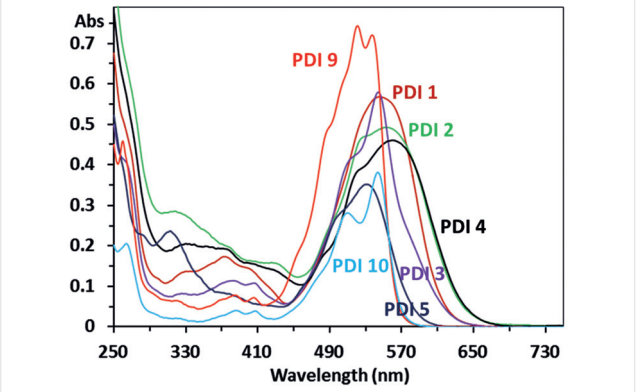

Figure 4 The UV–vis spectra of PDIs **1**–**5**, **9**, and **10** recorded in MeCN

We assumed that the broadening of the absorption spectra of the dissymmetric substituted PDIs was due to either a large twist angle of the naphthalene rings of the PDI moiety, induced by the presence of substituents, or to an increase in conjugation between the donor substituent and the PDI moiety. However, on moving from PDI **9** to PDIs **1** and **2**, a minor red shift was observed (Table 1), so it is probable that twisting of the naphthalene rings in the PDI moiety is responsible for the spectral broadening and the decrease in conjugation. Despite the greater angles between the two naphthalene units of the perylenediimide moieties in **1**–**4**, the bathochromic shift in the absorption spectrum might be attributable to internal charge transfer.

In conclusion, we have synthesized and characterized the novel dissymmetric *bay*-substituted PDIs **1** – **5**, which might find potential applications in several fields, for example, as reaction-based near-IR colorimetric probes or in the development of long-wavelength-absorbing dyes.

Funding Information

This work was supported by CSIR [02(0267)/16/EMR-II] and DST-SERB (EMR/2016/002239) grants.

Acknowledgment

We thank UGC for the UPE program to the university and CAS status to the department and DST for the FIST program. K.K. is grateful to DST-SERB for a JRF fellowship.

Supporting Information

Supporting information for this article is available online at https://doi.org/10.1055/s-0037-1610186.

References and Notes

(1) Würthner, F. *Chem. Commun.* **2004**, 1564.
(2) (a) Würthner, F.; Saha-Möller, C. R.; Fimmel, B.; Ogi, S.; Leowanawat, P.; Schmidt, D. *Chem. Rev.* **2016**, *116*, 962. (b) Langhals, H. *Heterocycles* **1995**, *40*, 477.
(3) Huang, C.; Barlow, S.; Marder, S. R. *J. Org. Chem.* **2011**, *76*, 2386.
(4) (a) *Supramolecular Dye Chemistry*; Würthner, F., Ed.; Springer: Berlin, **2005**. (b) Sun, M.; Müllen, K.; Yin, M. *Chem. Soc. Rev.* **2016**, *45*, 1513.
(5) (a) Herbst, W.; Hunger, K. *Industrial Organic Pigments: Production, Properties, Applications*, 3rd ed.; Wiley-VCH: Weinheim, **2006**. (b) *High Performance Pigments*; Smith, H. M., Ed.; Wiley-VCH: Weinheim, **2003**.
(6) (a) Zhan, X.; Facchetti, A.; Barlow, S.; Marks, T. J.; Ratner, M. A.; Wasielewski, M. R.; Marder, S. R. *Adv. Mater. (Weinheim, Ger.)* **2011**, *23*, 268. (b) Li, C.; Wonneberger, H. *Adv. Mater. (Weinheim, Ger.)* **2012**, *24*, 613.
(7) Fernández-Lázaro, F.; Zink-Lorre, N.; Sastre-Santos, A. *J. Mater. Chem. A* **2016**, *4*, 9336.
(8) Li, G.; Zhao, Y.; Li, J.; Cao, J.; Zhu, J.; Sun, X. W.; Zhang, Q. *J. Org. Chem.* **2015**, *80*, 196.

(9) Mende, L. S.; Fechtenkötter, A.; Müllen, K.; Moons, E.; Frienda, R. H.; MacKenzie, J. D. *Science* **2001**, *293*, 1119.
(10) (a) Ford, W. E.; Kamat, P. V. *J. Phys. Chem.* **1987**, *91*, 6373. (b) Guo, X.; Facchetti, A.; Marks, T. J. *Chem. Rev.* **2014**, *114*, 8943.
(11) (a) Singh, P.; Mittal, L. S.; Kaur, S.; Kaur, S.; Bhargava, G.; Kumar, S. *Sens. Actuators, B* **2018**, *255*, 478. (b) Singh, P.; Mittal, L. S.; Singh, H.; Bhargava, G.; Kumar, S. *New J. Chem.* **2017**, *41*, 10281. (c) Singh, P.; Mittal, L. S.; Bhargava, G.; Kumar, S. *Chem. Asian J.* **2017**, *12*, 890.
(12) (a) Kumar, K.; Bhargava, G.; Kumar, S.; Singh, P. *New J. Chem.* **2018**, *42*, 1010. (b) Singh, P.; Kumar, K.; Bhargava, G.; Kumar, S. *J. Mater. Chem. C* **2016**, *4*, 2488. (c) Singh, P.; Mittal, L. S.; Vanita, V.; Kumar, K.; Walia, A.; Bhargava, G.; Kumar, S. *J. Mater. Chem. B* **2016**, *4*, 3750.
(13) (a) Singh, P.; Mittal, L. S.; Vanita, V.; Kumar, R.; Bhargava, G.; Walia, A.; Kumar, S. *Chem. Commun.* **2014**, *50*, 13994. (b) Singh, P.; Mittal, L. S.; Kumar, S.; Bhargava, G.; Kumar, S. *J. Fluoresc.* **2014**, *24*, 909.
(14) (a) Marcia, M.; Singh, P.; Hauke, F.; Maggini, M.; Hirsch, A. *Org. Biomol. Chem.* **2014**, *12*, 7045. (b) Weißenstein, A.; Würthner, F. *Chem. Commun.* **2015**, *51*, 3415.
(15) (a) Grisci, G.; Mróz, W.; Catellani, M.; Kozma, E.; Galeotti, F. *ChemistrySelect* **2016**, *1*, 3033. (b) Cheng, H.-r.; Qian, Y. *Sens. Actuators, B* **2015**, *219*, 57.
(16) (a) Che, Y.; Yang, X.; Zang, L. *Chem. Commun.* **2008**, 1413. (b) Zhou, R.; Li, B.; Wu, N.; Gao, G.; You, J.; Lan, J. *Chem. Commun.* **2011**, *47*, 6668.
(17) (a) Liu, K.; Xu, Z.; Yin, M.; Yang, W.; He, B.; Wei, W.; Shen, J. *J. Mater. Chem. B* **2014**, *2*, 2093. (b) Sukul, P. K.; Santra, D. C.; Singh, P. K.; Maji, S. K.; Malik, S. *New J. Chem.* **2015**, *39*, 5084. (c) Dwivedi, A. K.; Pandeeswar, M.; Govindaraju, T. *ACS Appl. Mater. Interfaces* **2014**, *6*, 21369.
(18) (a) Fabian, J.; Nakazumi, H.; Matsuoka, M. *Chem. Rev.* **1992**, *92*, 1197. (b) Lin, M.-J.; Fimmel, B.; Radacki, K.; Würthner, F. *Angew. Chem. Int. Ed.* **2011**, *50*, 10847.
(19) (a) Liu, X.; Cai, Y.; Huang, X.; Zhang, R.; Sun, X. *J. Mater. Chem. C* **2017**, *5*, 3188. (b) Liu, Z.; Wu, Y.; Zhang, Q.; Gao, X. *J. Mater. Chem. A* **2016**, *4*, 17604.
(20) (a) Li, Y.; Qing, Z.; Yu, Y.; Liu, T.; Jiang, R.; Li, Y. *Chem. Asian J.* **2012**, *7*, 1934. (b) Li, Y.; Zheng, H.; Li, Y.; Wang, S.; Wu, Z.; Liu, P.; Gao, Z.; Liu, H.; Zhu, D. *J. Org. Chem.* **2007**, *72*, 2878.
(21) (a) Wang, R.; Li, G.; Zhang, A.; Wang, W.; Cui, G.; Zhao, J.; Shi, Z.; Tang, B. *Chem. Commun.* **2017**, *53*, 6918. (b) Tsai, H.-Y.; Chang, C.-W.; Chen, K.-Y. *Molecules* **2014**, *19*, 327.
(22) (a) Singh, P.; Singh, H.; Vanita, V.; Sharma, R.; Bhargava, G.; Kumar, S. *ChemistrySelect* **2016**, *1*, 6880. (b) Singh, P.; Singh, H.; Sharma, R.; Bhargava, G.; Kumar, S. *J. Mater. Chem. C* **2016**, *4*, 11180. (c) Singh, P.; Singh, H.; Sharma, R.; Dhawan, S.; Singh, P.; Bhargava, G.; Kumar, S. *J. Photochem. Photobiol., A* **2018**, *353*, 150.
(23) (a) Rajasingh, P.; Cohen, R.; Shirman, E.; Shimur, L. J. W.; Rybtchinski, B. *J. Org. Chem.* **2007**, *72*, 5973. (b) Chen, K.-Y.; Chow, T. J. *Tetrahedron Lett.* **2010**, *51*, 5959.

(24) **Dissymmetric Trisubstituted PDI 2; Typical Procedure**
PDI **9** (300 mg, 0.51 mmol) was dissolved in CH_2Cl_2 (30 mL). HNO_3 (771.56 µL, 8.60 mmol), CAN (280 mg, 0.51 mmol), and H_2SO_4 (984.95 µL, 9.65 mmol) were added, and the mixture was stirred at r.t. for 10 h. When the reaction was complete (TLC), H_2O was added to the mixture and the organic layer was repeatedly extracted with water (pH 7.0), dried (Na_2SO_4), and concentrated. The crude product was purified by column chromatography (silica gel, 70% $CHCl_3$–hexane).

(25) **PDI 2**
Dark-blue solid; yield: 316 mg (0.468 mmol, 91.3%); R_f = 0.40 ($CHCl_3$–hexane, 7:3). IR (ATR): 3287, 2966, 2933, 2875, 2360, 2126, 1701, 1661, 1595, 1543, 1459, 1411, 1357, 1313, 1250, 1200, 1070, 999, 928, 809 cm^{-1}. ^1H NMR (500 MHz, $CDCl_3$, 25 °C): δ = 9.12 (s, 1 H, perylene ArH), 8.85 (s, 1 H, perylene ArH), 8.55 (d, *J* = 8.0 Hz, 1 H, perylene ArH), 8.53 (s, 1 H, perylene ArH), 8.30 (d, *J* = 8.0 Hz, 1 H, perylene ArH), 5.07 (d, *J* = 2.0 Hz, 2 H, OCH_2), 5.01–5.06 (m, 2 H, ethylpropyl), 2.69 (t, *J* = 2.5 Hz, 1 H, –C≡H), 2.21–2.27 (m, 4 H, ethylpropyl), 1.92–1.98 (m, 4 H, ethylpropyl), 0.91 (t, *J* = 7.5 Hz, 6 H, ethylpropyl), 0.94 (t, *J* = 7.5 Hz, 6 H, ethylpropyl). ^{13}C NMR (125 MHz, $CDCl_3$, 25 °C): δ = 11.23, 11.35, 24.84, 25.03, 56.92, 58.35, 58.60, 75.76, 78.60, 116.31, 123.77, 126.68, 127.10, 127.44, 128.11, 129.56, 129.75, 148.07, 148.61, 157.79. Emission = 536 nm; Absorption = 561 nm (MeCN–H_2O with f_w = 50 vol%).

(26) **Dissymmetric Disubstituted PDI 1; General Procedure**
PDI **9** (50 mg, 0.085 mmol) was dissolved in CH_2Cl_2 (5 mL). HNO_3 (42.86 µL, 0.48 mmol), CAN (22.22 mg, 0.04 mmol), and H_2SO_4 (22.80 µL, 0.21 mmol) were added, and the mixture was stirred at r.t. for 4 h. When the reaction was complete (TLC), H_2O was added to the mixture and the organic layer was repeatedly extracted with H_2O (pH 7.0), dried (Na_2SO_4), and concentrated. The crude product was purified by column chromatography (silica gel, 70% $CHCl_3$–hexane).

(27) **PDI 1**
Dark-purple solid; yield: 48.2 mg (0.076 mmol, 89.6%); R_f = 0.26 ($CHCl_3$–hexane, 7:3); IR (ATR): 3265, 2924, 2853, 2361, 1699, 1659, 1594, 1461, 1412, 1315, 1251, 1070, 808, 743 cm^{-1}. ^1H NMR (500 MHz, $CDCl_3$, 25 °C): δ = 9.05 (s, 1 H, perylene ArH), 8.78 (d, *J* = 8.0 Hz, 1 H, perylene ArH), 8.68 (d, *J* = 8.0 Hz, 1 H, perylene ArH), 8.64 (d, *J* = 8.0 Hz, 2 H, perylene ArH), 8.51 (s, 1 H, perylene ArH), 5.06–5.10 (m, 2 H, ethylpropyl), 5.05 (d, *J* = 2 Hz, 2 H, OCH_2), 2.66 (t, *J* = 2.5 Hz, 1 H, –C≡H), 2.21–2.30 (m, 4 H, ethylpropyl), 1.90–1.99 (m, 4 H, ethylpropyl), 0.90–0.95 (m, 12 H, ethylpropyl). ^{13}C NMR (125 MHz, $CDCl_3$, 25 °C): δ = 11.28, 11.35, 24.93, 25.04, 56.64, 58.05, 58.09, 76.14, 78.17, 117.84, 123.43, 124.30, 124.76, 126.88, 128.08, 128.45, 129.67, 132.15, 135.41, 148.04, 156.62. Emission = 542 nm; Absorption = 560 nm (MeCN–H_2O with f_w = 50 vol%).

(28) **PDI 3**
Dark-purple solid; yield: 50.7 mg (0.078 mmol, 94.3%); R_f = 0.20 ($CHCl_3$–hexane, 7:3). IR (ATR): 3453, 3301, 2964, 2874, 2360, 1698, 1658, 1593, 1537, 1460, 1415, 1314, 1264, 1201, 1071, 988, 850, 809, 744 cm^{-1}. ^1H NMR (400 MHz, $CDCl_3$, 25 °C): δ = 9.08 (s, 1 H, perylene ArH), 8.79 (d, *J* = 9.6 Hz, 1 H, perylene ArH), 8.60–8.72 (m, 3 H, perylene ArH), 8.36 (s, 1 H, perylene ArH), 5.03–5.11 (m, 2 H, ethylpropyl), 4.49 (t, *J* = 9.6 Hz, 2 H, –OCH_2), 2.81 (td, *J* = 9.6, 3.2 Hz, 2 H, –CH_2), 2.19–2.34 (m, 4 H, ethylpropyl), 1.87–2.01 (m, 5 H, merged –CH + ethylpropyl), 0.90–0.96 (m, 12 H, ethylpropyl). ^{13}C NMR (125 MHz, $CDCl_3$): δ = 11.26, 11.28, 24.89, 25.01, 29.71, 57.94, 58.08, 58.23, 58.38, 128.83, 129.00, 129.55, 129.82, 131.29, 131.54, 141.03, 147.65, 147.82. Emission = 540 nm; Absorption = 550 nm (MeCN–H_2O with f_w = 50 vol%).

(29) **PDI 4**
Dark-blue solid; yield: 54.2 mg (0.079 mmol, 94.3%); R_f = 0.27 ($CHCl_3$–hexane, 7:3). IR (ATR): 3452, 3301, 3061, 2961, 2926, 2873, 2360, 1702, 1662, 1597, 1541, 1459, 1419, 1344, 1314, 1268, 1201, 1073, 1004, 926, 810, 742, 652 cm^{-1}. ^1H NMR (400 MHz, $CDCl_3$, 25 °C): δ = 9.15 (s, 1 H, perylene ArH), 8.85 (s, 1 H, perylene ArH), 8.54 (d, *J* = 8.0 Hz, 1 H, perylene ArH), 8.39 (s, 1 H, perylene ArH), 8.30 (d, *J* = 8.0 Hz, 1 H, perylene ArH), 5.00–

5.10 (m, 2 H, ethylpropyl), 4.53 (t, J = 7.2 Hz, 2 H, $-OCH_2$), 2.81 (td, J = 7.2, 2.4 Hz, 2 H, $-CH_2$), 2.19–2.30 (m, 4 H, ethylpropyl), 1.99 (t, J = 2.8 Hz, 1 H, –CH), 1.89–1.98 (m, 4 H, ethylpropyl), 0.90–0.95 (m, 12 H, ethylpropyl). ^{13}C NMR (125 MHz, $CDCl_3$): δ = 11.26, 11.32, 18.94, 24.86, 25.04, 58.36, 58.63, 68.04, 71.02, 78.76, 116.01, 123.54, 126.60, 127.53, 129.64, 129.80, 148.03, 159.02. Emission = 541 nm; Absorption = 565 nm (MeCN–H_2O with f_w = 50 vol%).

(30) **PDI 5**

Brownish-red liquid; yield: 102.1 mg (0.15 mmol, 95.2%); R_f = 0.23 ($CHCl_3$–hexane, 7:3). ^{1}H NMR (500 MHz, $CDCl_3$, 25 °C): δ = 10.15 (s, 1 H, CHO), 8.82 (s, 1 H, perylene ArH), 8.66 (t, J = 10.0 Hz, 2 H, perylene ArH), 8.24 (d, J = 10.0 Hz, 2 H, perylene-ArH), 8.06 (d, J = 10.0 Hz, 2 H, ArH), 7.82 (d, J = 10.0 Hz, 1 H, perylene ArH), 7.74 (d, J = 10.0 Hz, 1 H, ArH), 7.66 (d, J = 10.0 Hz, 1 H, ArH), 5.01–5.06 (m, 2 H, ethylpropyl), 2.19–2.28 (m, 4 H, ethylpropyl), 1.88–1.96 (m, 4 H, ethylpropyl), 0.87–0.94 (m, 12 H, ethylpropyl). ^{13}C NMR (125 MHz, $CDCl_3$): δ = 191.2, 147.9, 147.7, 141.0, 136.4, 134.9, 131.6, 131.3, 129.9, 129.6, 129.0, 128.9, 128.1, 58.4, 58.3, 58.1, 58.0, 36.9, 29.7, 25.0, 24.9, 19.2, 11.3, 11.3.

(31) Mishra, A.; Nayak, P. K.; Ray, D.; Patankar, M. P.; Narasimhan, K. L.; Periasamy, N. *Tetrahedron Lett.* **2006**, *47*, 4715.